Decoding face recognition abilities in the human brain

Faghel-Soubeyrand, Simon; Ramon, Meike; Bamps, Eva; Zoia, Matteo; Woodhams, Jessica; Richoz, Anne-Raphaelle; Caldara, Roberto; Gosselin, Frederic; Charest, Ian

DOI:
10.1093/pnasnexus/pgae095

Decoding face recognition abilities in the human brain

Simon Faghel-Soubeyrand [1,2], Meike Ramon[3], Eva Bamps [5], Matteo Zoia [6], Jessica Woodhams [2], Anne-Raphaelle Richoz[4], Roberto Caldara[4], Frédéric Gosselin[2] & Ian Charest [2]

1. Department of Experimental Psychology, University of Oxford, UK
2. Département de psychologie, Université de Montréal, Canada
3. Institute of Psychology, University of Lausanne, Switzerland
4. Département de Psychology, Université de Fribourg, Switzerland
5. Center for Contextual Psychiatry, Department of Neurosciences, KU Leuven, Belgium
6. Department for Biomedical Research, University of Bern, Switzerland

Corresponding authors:
Ian Charest,
ian.charest@umontreal.ca
Simon Faghel-Soubeyrand,
simon.faghel-soubeyrand@psy.ox.ac.uk

Significance

The ability to robustly recognise faces is crucial to our success as social beings. Yet, we still know very little about the brain mechanisms allowing some individuals to excel at face recognition. This study builds on a sizeable neural dataset measuring the brain activity of individuals with extraordinary face recognition abilities—super-recognisers—to tackle this challenge. Using state-of-the-art computational methods, we show robust prediction of face recognition abilities in single individuals from a mere second of brain activity, and reveal specific brain computations supporting individual differences in face recognition ability. Doing so, we provide direct empirical evidence for an association between semantic computations and face recognition abilities in the human brain—a key component of prominent face recognition models.

Abstract

Why are some individuals better at recognising faces? Uncovering the neural mechanisms supporting face recognition ability has proven elusive. To tackle this challenge, we used a multi-modal data-driven approach combining neuroimaging, computational modelling, and behavioural tests. We recorded the high-density electroencephalographic brain activity of individuals with extraordinary face recognition abilities—super-recognisers—and typical recognisers in response to diverse visual stimuli. Using multivariate pattern analyses, we

decoded face recognition abilities from 1 second of brain activity with up to 80% accuracy. To better understand the mechanisms subtending this decoding, we compared representations in the brains of our participants with those in artificial neural network models of vision and semantics, as well as with those involved in human judgments of shape and meaning similarity. Compared to typical recognisers, we found stronger associations between early brain representations of super-recognisers and mid-level representations of vision models as well as shape similarity judgments. Moreover, we found stronger associations between late brain representations of super-recognisers and representations of the artificial semantic model as well as meaning similarity judgments. Overall, these results indicate that important individual variations in brain processing, including neural computations extending beyond purely visual processes, support differences in face recognition abilities. They provide the first empirical evidence for an association between semantic computations and face recognition abilities. We believe that such multi-modal data-driven approaches will likely play a critical role in further revealing the complex nature of idiosyncratic face recognition in the human brain.

Introduction

The ability to robustly recognise the faces of our colleagues, friends and family members is paramount to our success as social beings. Our brains complete this feat with apparent ease and speed, in a series of computations unfolding within tens of milliseconds in a wide brain network comprising the inferior occipital gyrus, the fusiform gyrus, the superior temporal sulcus, and more anterior areas such as the anterior temporal lobe (1–3). Accumulating neuropsychological and behavioural evidence indicates that not all individuals, however, are equally competent at recognising faces in their surroundings (4). Developmental prosopagnosics show a great difficulty at this task despite an absence of brain injury (5). In contrast, super-recognisers exhibit remarkable abilities for processing facial identity, and can recognize individuals even after little exposure several years before (6–8). The specific nature of the neural processes responsible for these individual differences remains largely unknown. So far, individual differences studies have used univariate techniques to investigate face-specific aspects of brain processing. This revealed that contrasts between responses to faces compared to non-faces, measured by the N170 event-related potential component or by the blood oxygen level dependent signals in regions of interest, are modulated by ability (9–15). However, univariate and contrast approaches are limited in their capacity to reveal the precise nature of the underlying brain computations (16–19).

Here, we tackled this challenge with a data-driven approach. We examined the functional differences between the brains of super-recognisers and typical recognisers using decoding and representational similarity analyses (RSA; (18, 20–23)) applied to high-density electrophysiological (EEG) signals and artificial neural network models. We recruited 33 participants, including 16 super-recognisers, i.e., individuals better than the 98th percentile on a battery of face recognition tests (8); **Fig. 1a**). We measured EEG in more than 100,000 trials while participants performed a one-back task. The objects depicted in the stimuli belonged to

multiple visual categories including face images of different sexes, emotions, and identities, as well as images of man-made and non-face natural objects (e.g., a computer, a plant), animals (e.g., a giraffe, a monkey), and scenes (e.g., a city, a dining room; **Fig. 1b**).

Results

Behavioural results

All participants' face recognition ability was assessed using the Cambridge Face Memory Test long-form (CFMT+, (8). Scores on the CFMT+ ranged from 50 to 85 in the typical recognisers group (M_{TRs}=70.00; SD=9.09), and from 92 to 100 in the experimental super-recogniser group (M_{SRs}=95.38, SD=2.68; difference between groups : $t(31)=10.6958$, $p<.00001$ see Fig. 1a). The main experimental task was a one-back task (Fig. 1b). Accuracy was significantly greater for the super-recognisers (M_{SRs}=.8649, SD=.0626) than for the typical recognisers (M_{TRs}=.7591, SD=.096; $t(30)=3.6131$, p=.0011). This was also true when analysing separately face (M_{SRs}= .8677, SD=.0590; M_{TRs}=.7385, SD=.1048; $t(30)=4.2180$, p=.00020) and non-face trials (M_{SRs}=.8619, SD=.0750; M_{TRs}=.7798, SD=.1000; $t(30)=2.6000$, p=.0143). Furthermore, accuracy in the one-back task was positively correlated with scores on the CFMT+ (r=.68, $p<.001$; RT was marginally associated with CFMT+, r=.37, p=.04). We observed a significant difference in response times between the two groups for face stimuli (M_{SRs}=0.6222 ms, SD=.1386 ms; M_{TRs}= 0.6817 ms, SD=.0660 ms; p = 0.0258) but not for non-face stimuli (M_{SRs}=0.6262 ms, SD=.1401 ms; M_{TRs}= 0.6739 ms, SD=.0643 ms; p = .0801).

Discriminating super-recognisers and typical recognisers from 1 second of brain activity

With this sizable and category-rich dataset, we first attempted to classify a participant as either a super- or a typical recogniser based solely on their brain activity. More specifically, we trained Fisher linear discriminants to predict group membership from single, 1-second trials of EEG patterns (in a moving searchlight of five neighbouring electrodes; **Fig. 2b**). We observed up to ~80% cross-validated decoding performance, peaking over electrodes in the right hemisphere. This performance is impressive given that the noise ceiling imposed on our classification by the test-retest reliability of the CFMT+ (8, 24), the gold-standard test used to identify super-recogniser individuals, is ~93% (SD=2.28%; see Supplementary material). To reveal the time course of these functional differences, we applied the same decoding procedure to each 4-ms interval of EEG recordings. Group-membership predictions attained statistical significance ($p<.001$, permutation tests, **Fig. 2a**) from about 65 ms to at least 1 s after stimulus onset, peaking around 135 ms, within the N170 window (25, 26).

Notably, similar results were obtained following the presentation of both face *and* non-face visual stimuli (**Fig. 2a; see also Figure S1**). This did not result from face representations stored in short-term memory from one-back trials. Indeed, we repeated our decoding analysis for non-face trials either preceded by face trials or by non-face trials, and found significant

decoding of group membership in both cases (**Figure S1**). In addition, we successfully cross-decoded group membership from a model trained on face EEG activity and applied to non-face EEG activity (**see Figure S2)**. The decoding of group-membership could be based on various features. Some of these features are directly related to brain representations for object and face recognition, and these aspects are further explored in subsequent sections of this article. On the other hand, there could be additional contributing features that are not directly linked to object and face recognition. For instance, differences in motor responses between the two subject groups might explain these results to some extent. However, excluding the 10% of trials with a motor response did not affect decoding accuracy (**Figure S2**). Additionally, the decoding model might have relied on potential noise differences between the two subject groups. Nevertheless, our analysis did not reveal any evidence supporting such differences in the cross-participant similarity of the Representational Dissimilarity Matrices (RDMs) for both groups (see section Linking neural representations with computational models of vision; **Figure S3**).

Predicting individual recognition ability from 1 second of brain activity

An ongoing debate in individual differences research is whether the observed effects emerge from qualitative or quantitative changes in the supporting brain mechanisms (27–35). The decoding results presented up to this point might give the impression that face recognition ability is supported by qualitative differences in brain mechanisms. However, these results were obtained with dichotomous classification models applied, by design, to the brains of individuals from a bimodal distribution of ability scores (e.g. (32).

To better assess the nature of the relationship between neural representations and ability in the general population, we thus performed a new decoding analysis on the typical recognisers only, using a continuous regression model. Specifically, we used cross-validated fractional ridge regression (36) to predict *individual* CFMT+ face recognition ability scores from single-trial EEG data. This showed essentially similar results to the previous dichotomic decoding results: performance was above statistical threshold (p<.01, FDR-corrected) from about 80 ms to at least 1 s, peaking around 135 ms following stimulus onset for both face and non-face stimuli (**Fig. 2c,** peak-rho$_{face}$=.4149 at 133 ms, peak-rho$_{non\text{-}face}$=.4899 at 141 ms). This accurate decoding of individual scores from EEG patterns is compatible with a quantitative account of variations in brain mechanisms across individuals differing in face recognition abilities. Altogether, these decoding results provide evidence for important, quantitative and temporally extended variations in the brain activity supporting face recognition abilities. This extended decoding suggests effects of individual ability across multiple successive processing stages.

Linking neural representations with computational models of vision

Decoding time courses, however, offer limited insights on the level of brain computations (37, 38). To better characterise the visual brain computations covarying with face recognition ability, we compared, using representational similarity analysis (20–22, 39), the brain

representations of our participants to that of convolutional neural networks (CNNs) trained to categorise objects (40–42). These CNNs process visual features of gradually higher complexity and abstraction along their layers (42), from low-level (e.g., orientation, edges) to high-level features (e.g., objects and object parts).

The brain representations were characterised by computing representational dissimilarity matrices (RDMs) for each participant and for each 4-ms time interval. These brain RDMs were derived using the cross-validated decoding performance of a linear discriminant model, where brain activity was decoded for every pair of stimuli at a given time interval (43, 44); see **Figure S4** for the group-average RDMs and time course of key categorical distinctions). The visual model representations were characterised by computing RDMs from the layers of the CNNs, using Pearson correlations of the unit activations across all pairs of stimuli. Compared to typical participants, we found that the brain RDMs of super-recognisers showed larger mutual information (45) with the layer RDMs of CNNs that represent mid-level features (e.g., combinations of edges, contour, shape, texture; (42, 46) between 133 and 165 ms (**Fig. 3a**, $p<.05$, cluster-test; see also **Figure S5** for similar results with unconstrained analyses; supplementary analyses on specific category conditions in the RDMs are shown on **Figure S6**). These results indicate that mid-level representations of an object-trained CNN matched the representations of super-recognisers more closely than those of typical participants. We replicated these results using a face-trained CNN (e.g., (47–49), VGGface (50), which possess mid-level representations similar to those of object-trained CNN (see **Figure S7**; $p<.05$, cluster-test). The stronger association between brain representational geometries of the super-recognisers with computational models of vision could be explained by a marked difference in signal to noise between the two groups of participants. To control for this potential confound, we computed the cross-participant similarity of the RDMs in both groups (see **Figure S3**). If the signal to noise was larger in the super-recognisers, we would expect larger cross-participant similarity of the RDMs, however, we observed no significant difference between the two groups.

Linking neural representations with computational model of semantics

The finding that ability decoding was significant as late as 1 s after stimulus onset hints that brain computations beyond what is typically construed as pure visual processing also differ as a function of face recognition ability. To test this hypothesis, we asked five new participants to write captions describing the images presented during our experiment (e.g., “A city seen through a forest.”), and used a deep averaging network (Google Universal Sentence Encoder, GUSE; (51) to transform these captions into embeddings (points in a caption space). GUSE has been trained to predict semantic textual similarity from human judgments, and its embeddings generalise to an array of other semantic judgement tasks (51). We then compared the RDMs computed from this semantic model to the brain RDMs of both typical- and super-recognisers. Importantly, both this comparison, and the one comparing brain and visual models, excluded the information shared between the semantic and visual models (but see

Figure S8 for similar results with unconstrained analyses). We found larger mutual information with these semantic representations in the brains of super-recognisers than in those of typical recognisers in a late window between 598 and 727 ms (**Fig. 3b**, $p<.05$, cluster-test). Supplementary analyses on specific stimulus categories of the RDMs (**Figure S9**) suggest that these results emerged mainly from the face-vs-face and face-vs-non-face stimuli pair conditions.

Linking neural representations with behavioural representations for shape and semantic similarity judgements

Our findings so far suggest that mid-level visual and semantic brain processes both support individual differences in face recognition abilities. We looked for further support for these conclusions using RDMs derived from a behavioural experiment. A group of 32 new human participants were submitted to two multiple arrangement tasks (52–54) in which they were asked to evaluate the shape similarities of all pairs of the 49 visual stimuli used in the main experiment, and the meaning similarities of all pairs of the 49 mean sentence captions produced by five human participants to describe these images and used for the semantic model (see section Linking neural representations with computational model of semantics). More specifically, participants arranged the images/sentences inside a white circular arena according to the task instructions using simple drag and drop operations (see **Fig. 4**). We computed the mutual information between the mean RDMs extracted from each of these tasks and the time-resolved brain RDMs of super- and typical recognisers as well as the same while excluding the information shared with the other task. Results indicated only a small trend for shape representations being enhanced around mid-latencies in super-recognisers relative to typical recognisers which did not survive cluster correction ($p<.01$, uncorrected; $p_{MI} = .1259$; $p_{CMI} = .2098$; cluster-corrected; see **Fig. 4**). Meaning representations were enhanced in late latencies in super-recognisers compared to typical recognisers (sentence meaning : 635-787 ms $p < .05$, cluster-corrected; see **Fig. 4**). These results confirm that semantic representations at relatively late latencies and, to a lesser degree, shape representations at mid latencies are enhanced in the brains of super-recognisers.

Discussion

Using a data-driven approach combining neuroimaging, computational models, and behavioural tests, we characterised the computations modulated by variations in face recognition ability in the human brain. We recorded high-density electroencephalographic (EEG) responses to face and non-face stimuli in super-recognisers and typical recognisers. Using multivariate analysis, we reliably decoded group membership as well as recognition abilities of single individuals from a single second of brain activity. We then characterised the neural computations underlying these individual differences by comparing human brain activity with representations from artificial neural network models of vision and semantics using

representational similarity analysis. Furthermore, we compared the brain activity with similarity judgments derived from additional human participants engaged in two tasks. In the first task, participants judged our visual stimuli on the similarity of their shape, while In the second task, participants judged sentence captions describing these stimuli on the similarity of their meaning. These sets of comparisons revealed two main findings. First, we found higher similarity between early brain representations of super-recognisers and mid-level representations of vision models as well as, to a lesser degree, shape similarity judgments. Second, this approach revealed higher similarity between late brain representations of super-recognisers and representations of an artificial semantic model as well as sentence caption similarity judgments. To our knowledge, this is the first demonstration of a link between face recognition ability and brain computations beyond high-level vision. Overall, these findings revealed specific computations supporting our individual ability to recognise faces, and suggest widespread variations in brain processes related to this crucial ability.

We achieved robust decoding of face recognition ability when examining EEG responses to face *and* non-face stimuli. This is consistent with several neuropsychological (30, 55–59) and brain imaging findings (12, 29, 60, 61) showing face and non-face processing effects in individuals across the spectrum of face recognition ability ((19, 62); but see (13, 63–65)).

The decoding we observed for face and non-face stimuli peaked at right occipito-temporal electrodes, in the temporal window around the N170 component (25). At that time, the representations in the brains of our participants differed most with respect to the mid-layer representations of artificial models of vision. These layers have been previously linked to processing in human infero-temporal cortex (hIT; (42, 66–68) and functionally to mid-level feature representations such as combinations of edges and parts of objects (42, 46). Such associations with the N170, however, do not mean that this component is exclusively involved in these mid-level processes. Rather, it suggests that other visual computations, including the high-level visual computations usually associated with the N170, do not differ substantially between super-recognisers and typical recognisers. The fact that these mid-level features are mostly shared between face and non-face stimuli could explain at least partly the high decoding performance observed for both classes of stimuli. They suggest that a mid-level visual processing is enhanced in SRs leading to improved processing of faces and objects.

Crucially, we found that face recognition ability is also associated with semantic computations that extend beyond basic-level visual categorisation in a late time-window around the P600 component (69–71). Recent studies using computational techniques have shown that word representations derived from models of natural language processing explain significant variance in the visual ventral stream (18, 72–74). The current study goes beyond this recent work in two ways. First, our use of human sentence description and sentence encoders to characterise semantic (caption-level) computations provides a more abstract description of brain representations. Second, and most importantly, our work revealed a link between semantic brain computations and individual differences in face recognition ability. An association between semantic processes and face recognition ability had been posited in models of face recognition (1, 75) but, to our knowledge, it had never been shown empirically

before.

Overall, thus, our findings suggest important differences in perceptual and semantic representations in individuals with outstanding ability to recognise faces. The higher similarity with computational models of vision indicate that super-recognisers have more efficient mid-level representations. These enhanced representations suggest that part-based information about faces and objects, putatively emerging from mid-level occipito-temporal regions (76), is richer in individuals with strong face recognition abilities (77). Furthermore, our findings show that the more similar the brain representations of an individual are to task-optimised computational models of semantics, the better they are at recognising faces. These enhanced late semantic representations, for example, might emerge from enhanced subordinate-level information about objects and faces (78, 79).

Our approach of decoding group membership to reveal electrophysiological differences between super-recognisers and typical recognisers, followed by representational similarity analysis with computational models of vision and language, enabled revealing potential mechanisms underlying enhanced recognition ability. Other possible differences between our participants might also contribute to our ability to decode their brain signals. Differences in top-down (i.e. attention) mechanisms, better ability to memorise images more generally, or both, could also lead to enhanced representations. Interestingly, we could decode from both face *and* nonface categories, and across categories (training with face trials and testing on non-face trials) suggesting that the mechanisms subtending the enhanced abilities of super-recognisers are not restricted to faces (4), (56).

Furthermore, while our decoding approach indicates that important differences in brain processing emerge from early (80 ms) to late (~1s) processing windows, our RSA modelling approach only explained part of these processing windows. Specifically, while broad visual (~150 ms), face-specific (~430 ms), and semantic representations (~600 ms) were found to differ in super-recognisers using this computational approach, it still remains to be shown what specific representations are critical in differentiating the best face recognisers during early (<150 ms) and very late (>800 ms) windows of processing.

In conclusion, our results offer a stepping stone for a better understanding of face recognition idiosyncrasies in the human brain. Indeed, with the development of novel and better artificial models simulating an increasing variety of cognitive processes, and with the technological advances allowing the processing of increasingly larger neuroimaging datasets, the approach described here provides a new and promising way to tackle the link between individual differences in human behaviour and specific computations in the brain. In addition, this decoding approach may provide quick and accurate alternatives to standardised behavioural tests assessing face recognition ability, for example in the context of security settings that benefit from strong face processing skills among their personnel (such as police agencies, border patrol, etc.). It could also be used in a closed-loop training procedure designed to improve face recognition ability (80).

Methods

Participants

A total of 33 participants were recruited for this study. The first group consisted of 16 individuals with exceptional ability in face recognition — super-recognisers. The second group was composed of 17 neurotypical controls. These sample sizes were chosen according to the

effect sizes described in previous multivariate object recognition studies (43, 44, 54). The data from one super-recogniser was excluded due to faulty EEG recordings. No participant had a history of psychiatric diagnostic or neurological disorder. All had normal or corrected to normal vision. This study was approved by the Ethics and Research Committee of the University of Birmingham, and informed consent was obtained from all participants.

Sixteen previously known super-recognisers were tested in the current study (30-44 years old, 10 female). Eight of these (SR1-SR8) were identified by Prof. Josh Davis from the University of Greenwich using an online test battery comprising a total of six face cognition tasks (6) and tested at the University of Birmingham. The remaining eight (SR-9 to SR-16) were identified using three challenging face cognition tests (7) and were tested at the University of Fribourg. The behavioural test scores for all participants are provided in **Tables S1 and S2.** Across SR cohorts, the Cambridge Face Memory Test long-form (CFMT+; (8) was used as the measure of face identity processing ability. A score greater than 90 (i.e., 2 SD above average) is typically considered the threshold for super-recognition (8, 56, 81). Our 16 super-recognisers all scored above 92 (M=95.31; SD=2.68). A score of 92 corresponds to the 99th percentile according to our estimation from a group of 332 participants from the general population recruited in three independent studies (77, 82, 83).

An additional 17 typical recognisers (20-37 years old, 11 female) were recruited and tested on campus at the University of Fribourg (n=10) and the University of Birmingham (n=7). Their CFMT+ scores ranged from 50 to 85 (M=70.00; SD=9.08). Neither the average nor the distribution of this sample differed significantly from those of the 332 participants from the general population mentioned above (see **Fig. 1a**; t(346)=1.3065, p=0.1922; two-sample Kolmogorov-Smirnov test; D(346)=0.2545, p=0.2372).

Tasks

CFMT+

All participants were administered the CFMT long-form, or CFMT+ (8). In the CFMT+, participants are required to memorise a series of face identities, and to subsequently identify the newly learned faces among three faces. It includes a total of 102 trials of increasing difficulty. The duration of this test is about 15 minutes. EEG was not recorded while participants completed this test.

One-back task

Stimuli. The stimuli used in this study consisted of 49 images of faces, animals (e.g., giraffe, monkey, puppy), plants, objects (e.g., car, computer monitor, flower, banana), and scenes (e.g., city landscape, kitchen, bedroom). The 24 faces (13 identities, 8 males, and 8 neutral, 8 happy, 8 fearful expressions) were sampled from the Radboud Face dataset (84). The main facial features were aligned across faces using Procrustes transformations. Each face image was revealed through an ellipsoid mask that excluded non-facial cues. The non-face images were sampled from the stimulus set of Kiani et al. (85). All stimuli were converted to 250 x 250 pixels (8x8 deg of visual angle) greyscale images. The mean luminance and the luminance standard deviation of these stimuli were equalised using the SHINE toolbox (86).

Procedure. We measured high-density electroencephalographic (EEG; sampling rate = 1024 Hz; 128-channel BioSemi ActiveTwo headset) activity while participants performed ~3200 trials of a one-back task in two recording sessions separated by at least one day and by a maximum of two weeks (**Fig. 1b**). Participants were asked to press a computer keyboard key on trials where the current image was identical to the previous one. Repetitions occurred with a 0.1 probability. They were asked to respond as quickly and accurately as possible. Feedback was done in the form of a change in colour of the fixation point (red or green) after a repetition trial (which happened on a .1 probability basis). This was done to help participants pay attention during the task. Target trials were not excluded from the analyses. A trial unravelled as follows: a white fixation point was presented on a grey background for 500 ms (with a jitter of ± 50 ms); followed by a stimulus presented on a grey background for 600 ms; and, finally, by a white fixation point on a grey background for 500 ms. Participants had a maximum of 1100 ms following stimulus onset to respond. This interval, as well as the 200 ms preceding stimulus onset, constituted the epoch selected for our EEG analyses. In total, our participants completed 105,600 one-back trials which constituted ~32 hours of EEG epochs.

***Shape and sentence meaning multiple arrangements tasks*.** Thirty two new neurotypical participants took part in two multiple arrangements tasks (22, 87) in counterbalanced orders. In two of the tasks, they were asked to evaluate the shape or function similarities of the 49 stimuli used in the main experiment while, in the other task, they were instructed to judge the meaning similarities of sentence captions describing these stimuli (see Semantic Caption-level Deep Averaging Neural Network RDM for more information about these sentence captions).

More specifically, participants were asked to arrange stimuli or sentence captions on a computer screen inside a white circular arena by using computer mouse drag and drop operations. During the shape/function (vs. meaning) multiple arrangement task, they were instructed to place the displayed visual stimuli (vs. sentence captions) in such a way that their pairwise distances match their shape/function (vs. meaning) similarities as much as possible (**Fig. 4**). On the first trial of each task, participants arranged all 49 items. On subsequent trials, a subset of these items was selected based on an adaptive procedure aimed at minimising uncertainty for all possible pairs of items (e.g. items that initially were placed very close to each other) and at better approximating the high-dimensional perceptual representational space (87). This procedure was repeated until the task timed out (20 min).

We computed one RDM per task per participant. Three participants were excluded from the final sample because their RDMs differed from the mean RDMs by more than two standard deviations. Finally, we averaged the remaining individual RDMs within each task.

Analyses

All reported analyses were performed independently for each EEG recording session and then averaged. Analyses were completed using custom code written in MATLAB (MathWorks) and Python.

EEG preprocessing

EEG data was preprocessed using FieldTrip (88): continuous raw data was first re-referenced

relative to Cz, filtered with a band-pass filter [0.01-80 Hz], segmented into trial epochs from -200 ms to 1100 ms relative to stimulus onset, and down-sampled at 256 Hz.

Decoding analyses

Whole-brain analyses. To predict group-membership from EEG brain activity, we trained Fisher linear discriminant classifiers to predict participants' group membership based on raw EEG topographies, using all 128 channels of single-trial EEG data as features. Notably, here, the decoding is made on an *across-participants* basis. This was done across all trials of either face or non-face condition, for each of the two sessions separately (~26,000 observations per condition, per session, 5-fold cross-validation, 5 repetitions; (89, 90). The number of trials were matched across participants. This process was repeated over all EEG time samples separately, starting from -200 ms and ending 1100 ms after stimulus onset, creating decoding accuracy time courses. The Area Under the Curve (AUC) was used to assess sensitivity. Decoding time courses were averaged across the two EEG sessions. The resulting evidence indicates when super-recognisers can be categorised from brain activity when processing faces (blue) and non-face stimuli (grey), as shown in **Figure 2a**. Additional control decoding analyses investigating effects of one-back trials on the predictions are shown in **Figure S1.** These trials required that our participant compared their representations of the presented image and the one stored in short-term memory. This showed similar findings, with one notable difference being that the face-face discrimination condition was the one that obtained peak decoding accuracy.

Searchlight analysis. We conducted a searchlight analysis decoding EEG signals from all subsets of five neighbouring channels to characterise the scalp topographies of group-membership AUC. This searchlight analysis was done either using the entire EEG time series of a trial (0-1100 ms; **Fig. 2b,** leftmost topographies), or using 60 ms temporal windows (centred on 135 ms, 350 ms, 560 ms, and 775 ms; **Fig. 2b** rightmost topographies). We ran additional control searchlight decoding procedures investigating the effect of one-back trials (**Figure S1**).

Regression analysis. We used fractional ridge regression models (36) to predict individual face recognition ability scores (CFMT+) among the typical recognisers from EEG patterns across time. We trained our model on subsets of 60% of the EEG patterns. We chose the alpha hyperparameter with the best coefficient of determination among 20 alpha hyperparameters ranging linearly from 0.001 to 0.99 applied on a 30% validation set. The decoding performance was assessed using the Spearman correlation between the CFMT+ scores and predictions from the overall best model (applied on the remaining 10% of EEG patterns). This process was repeated 10 times and the Spearman correlations were averaged. Significance was assessed using a permutation test (see *Group comparisons and inferential statistics* section).

Representational Similarity Analysis of brain and computational models

We compared our participants' brain representations to those from visual and semantic (caption-level) artificial neural networks using Representational Similarity Analysis (RSA; (20–22, 39).

Brain Representational Dissimilarity Matrices. For every participant, we trained a Fisher linear discriminant to distinguish pairs of stimuli from every 4-ms intervals of EEG response (on all 128 channels) to these stimuli from -200 to 1100 ms after stimulus onset (91, 92). Cross-validated AUC served as pairwise classification dissimilarity metric. By repeating this process for all possible pairs (1176 for our 49 stimuli), we obtained a representational dissimilarity matrix (RDM). RDMs are shown for selected time points in **Figure S4**.

Visual Convolutional Neural Networks RDMs. We used a pre-trained AlexNet (40) as one model of the visual computations along the ventral stream (42). Our 49 stimuli were input to AlexNet. Layer-wise RDMs were constructed comparing the unit activation patterns for each pair of images using Pearson correlations. Similarly, we computed layer-wise RDMs from another well-known CNN, VGG-16 (see **Figure S5**). Following previous studies using this model (93, 94), we averaged the convolutional layer RDMs situated between each max pooling layers and the layers' input into five aggregated convolutional RDMs (e.g. conv1-1 & conv1-2 into RDM-conv1); this facilitated the comparison of our results with the five convolutional layers of AlexNet.

Semantic Caption-level Deep Averaging Neural Network RDM. We asked five new participants to provide a sentence caption describing each stimulus (e.g., "a city seen from the other side of the forest", see **Fig. 1d**) using the Meadows online platform (www.meadows-research.com). The sentence captions were input in Google's universal sentence encoder (GUSE; (51) resulting in 512 dimensional sentence embeddings for each stimulus. We then computed the dissimilarities (cosine distances) between the sentence embeddings across all pairs of captions, resulting in a semantic caption-level RDM for each participant. The average RDM was used for further analyses.

Comparing brain representations with computational models

We compared our participants' brain RDMs to those from the vision (Fig. 3a) and semantic (Fig. 3b) models described in the previous section using Conditional Mutual Information (45), which measures the statistical dependence between two variables (e.g. mutual information *I*(x;y)), removing the effect from a third variable (i.e. I(x;y|z)). Additional comparisons using unconstrained Mutual Information between brain RDMs and both models are shown in **Figure S5 and S8.**

Group comparison and inferential statistics

***Comparison of Conditional Mutual Information time courses*.** Time courses of CMI were compared between the super-recognisers and typical recognisers using independent samples t-tests and a Monte Carlo procedure at a *p-value* of .05, as implemented in the Fieldtrip Toolbox (88). Family-wise errors were controlled for using cluster-based corrections, with maximum cluster size as cluster-level statistic and an arbitrary *t* threshold for cluster statistic of [-1.96, 1.96] for the comparison of brain and semantic (excluding CNN) and for the comparison of brain and CNN (excluding semantic) time courses. The standard error is shown for all curves as colour-shaded areas (**Fig. 3**). Analyses with MI (brain; CNN) and MI (brain; semantic) were completed in an identical manner.

***Time course of group-membership decoding*.** Significance was assessed using non-parametric permutation tests. We simulated the null hypothesis by training the linear classifier to identify shuffled group-membership labels from the experimental EEG patterns. This process was repeated 1000 times for each time point and each one of the two sessions. We then compared the real, experimental decoding value at each time point to its corresponding null distribution, and rejected the null hypothesis if the decoding value was greater than the prescribed critical value at a p <.001 level.

***Time course of individual ability decoding using ridge regression*.** Significance was again assessed using non-parametric permutation testing. The ridge regression analysis predicted cross-validated CFMT+ scores from single trial EEG patterns, and goodness of fit is reported using Spearman's correlation between the predicted and observed CFMT+ scores. Under the null hypothesis that all participants elicited comparable EEG response patterns, irrespective of their CFMT+ score, the face recognition ability scores are exchangeable. We simulated this null hypothesis by repeating the ridge regression model training using randomly shuffled CFMT+ scores. The predicted CFMT+ scores were then correlated to the empirical, observed CFMT+ scores using Spearman's correlation, and this was repeated 1000 times for each time point. We finally compared the real, experimental correlation value with its corresponding null distribution at each time point, and rejected the null hypothesis if the correlation value was greater than the prescribed critical value at a p <.01 level.

Data availability

High-density EEG data associated with this article is available on The Open Science Framework (https://osf.io/pky28/).

Acknowledgements

We thank Prof. Josh P. Davis for sharing behavioural scores of super-recognisers and establishing first contact to the UK-based Super-Recognizers reported here. We also thank Mick Neville, from Super-Recognisers Ltd., who helped us to get in contact with some of our super-recognizer participants. We thank Rose Jutras, who helped with data acquisition. Funding for this project was supported by an ERC Starting Grant [ERC-StG-759432] to I.C, an ERSC-IAA grant to J.W., I.C. and S.F.S., by a Swiss National Science Foundation PRIMA (Promoting Women in Academia) grant [PR00P1_179872] to M.R., and by IVADO (2021-6707598907), NSERC, and UNIQUE graduate scholarships to S.F.S. This manuscript was posted on a preprint: https://www.biorxiv.org/content/10.1101/2022.03.19.484245v3. https://doi.org/10.1101/2022.03.19.484245

Author contributions
(CRediT standardised author statement)

S.F-S.: Conceptualisation, methodology, software, formal analysis, investigation, data curation, writing - original draft, visualisation, supervision, project administration, funding acquisition. **M.R.:** Investigation, resources, project administration, writing - review and editing. **E.B.:**

investigation, project administration. **M.Z.**: investigation. **J.W.:** funding acquisition, writing - review and editing. **A-R.R.**: Investigation. **R.C.:** Resources. **F.G.:** Methodology, writing - original draft, supervision, funding acquisition. **I.C.**: Supervision, methodology, software, resources, formal analysis, writing - original draft, project administration, funding acquisition.

Competing interests

The authors declare no competing interests.

References

1. B. Duchaine, G. Yovel, A Revised Neural Framework for Face Processing. *Annu Rev Vis Sci* **1**, 393–416 (2015).

2. N. Kanwisher, J. McDermott, M. M. Chun, The fusiform face area: a module in human extrastriate cortex specialized for face perception. *J. Neurosci.* **17**, 4302–4311 (1997).

3. K. Grill-Spector, K. S. Weiner, K. Kay, J. Gomez, The Functional Neuroanatomy of Human Face Perception. *Annu Rev Vis Sci* **3**, 167–196 (2017).

4. D. White, A. Mike Burton, Individual differences and the multidimensional nature of face perception. *Nature Reviews Psychology* (2022) https:/doi.org/10.1038/s44159-022-00041-3.

5. T. Susilo, B. Duchaine, Advances in developmental prosopagnosia research. *Current Opinion in Neurobiology* **23**, 423–429 (2013).

6. E. Noyes, J. P. Davis, N. Petrov, K. L. H. Gray, K. L. Ritchie, The effect of face masks and sunglasses on identity and expression recognition with super-recognizers and typical observers. *R Soc Open Sci* **8**, 201169 (2021).

7. M. Ramon, Super-Recognizers –a novel diagnostic framework, 70 cases, and guidelines for future work. *Neuropsychologia*, 107809 (2021).

8. R. Russell, B. Duchaine, K. Nakayama, Super-recognizers: people with extraordinary face recognition ability. *Psychon. Bull. Rev.* **16**, 252–257 (2009).

9. D. B. Elbich, S. Scherf, Beyond the FFA: Brain-behavior correspondences in face recognition abilities. *Neuroimage* **147**, 409–422 (2017).

10. G. Herzmann, O. Kunina, W. Sommer, Individual differences in face cognition: brain–behavior relationships. *Journal of Cognitive* (2010).

11. L. Huang, *et al.*, Individual differences in cortical face selectivity predict behavioral performance in face recognition. *Front. Hum. Neurosci.* **8**, 483 (2014).

12. L. Kaltwasser, A. Hildebrandt, G. Recio, O. Wilhelm, W. Sommer, Neurocognitive mechanisms of individual differences in face cognition: a replication and extension. *Cogn.*

Affect. Behav. Neurosci. **14**, 861–878 (2014).

13. M. Lohse, *et al.*, Effective Connectivity from Early Visual Cortex to Posterior Occipitotemporal Face Areas Supports Face Selectivity and Predicts Developmental Prosopagnosia. *J. Neurosci.* **36**, 3821–3828 (2016).

14. B. Rossion, T. L. Retter, J. Liu-Shuang, Understanding human individuation of unfamiliar faces with oddball fast periodic visual stimulation and electroencephalography. *Eur. J. Neurosci.* **52**, 4283–4344 (2020).

15. H. Nowparast Rostami, W. Sommer, C. Zhou, O. Wilhelm, A. Hildebrandt, Structural encoding processes contribute to individual differences in face and object cognition: Inferences from psychometric test performance and event-related brain potentials. *Cortex* **95**, 192–210 (2017).

16. K. Vinken, T. Konkle, M. Livingstone, The neural code for "face cells" is not face specific. *bioRxiv*, 2022.03.06.483186 (2022).

17. M. Visconti di Oleggio Castello, J. V. Haxby, M. I. Gobbini, Shared neural codes for visual and semantic information about familiar faces in a common representational space. *Proc. Natl. Acad. Sci. U. S. A.* **118** (2021).

18. K. Dwivedi, M. F. Bonner, R. M. Cichy, G. Roig, Unveiling functions of the visual cortex using task-specific deep neural networks. *PLoS Comput. Biol.* **17**, e1009267 (2021).

19. A. Harel, D. Kravitz, C. I. Baker, Beyond perceptual expertise: revisiting the neural substrates of expert object recognition. *Front. Hum. Neurosci.* **7**, 885 (2013).

20. N. Kriegeskorte, *et al.*, Matching categorical object representations in inferior temporal cortex of man and monkey. *Neuron* **60**, 1126–1141 (2008).

21. N. Kriegeskorte, R. A. Kievit, Representational geometry: integrating cognition, computation, and the brain. *Trends Cogn. Sci.* **17**, 401–412 (8/2013).

22. I. Charest, R. A. Kievit, T. W. Schmitz, D. Deca, N. Kriegeskorte, Unique semantic space in the brain of each beholder predicts perceived similarity. *Proceedings of the National Academy of Sciences* **111**, 14565–14570 (2014).

23. N. Kriegeskorte, J. Diedrichsen, Peeling the Onion of Brain Representations. *Annu. Rev. Neurosci.* **42**, 407–432 (2019).

24. B. Duchaine, K. Nakayama, The Cambridge Face Memory Test: Results for neurologically intact individuals and an investigation of its validity using inverted face stimuli and …. *Neuropsychologia* (2006).

25. S. Bentin, T. Allison, A. Puce, E. Perez, G. McCarthy, Electrophysiological studies of face perception in humans. *J. Cogn. Neurosci.* **8** (1996).

26. B. Rossion, C. Jacques, The N170: Understanding the time course of face perception in

the human brain. *The Oxford handbook of event-related potential components.* **641**, 115–141 (2012).

27. J. J. S. Barton, S. L. Corrow, The problem of being bad at faces. *Neuropsychologia* **89**, 119–124 (2016).

28. A. K. Bobak, B. A. Parris, N. J. Gregory, R. J. Bennetts, S. Bate, Eye-Movement Strategies in Developmental Prosopagnosia and "Super" Face Recognition. *Quarterly Journal of Experimental Psychology* **70**, 201–217 (2017).

29. G. Rosenthal, *et al.*, Altered topology of neural circuits in congenital prosopagnosia. *Elife* **6** (2017).

30. R. K. Hendel, R. Starrfelt, C. Gerlach, The good, the bad, and the average: Characterizing the relationship between face and object processing across the face recognition spectrum. *Neuropsychologia* **124**, 274–284 (2019).

31. E. K. Vogel, A. W. McCollough, M. G. Machizawa, Neural measures reveal individual differences in controlling access to working memory. *Nature* **438**, 500–503 (2005).

32. E. A. Maguire, E. R. Valentine, J. M. Wilding, N. Kapur, Routes to remembering: the brains behind superior memory. *Nat. Neurosci.* **6**, 90–95 (2003).

33. J. N. Zadelaar, *et al.*, Are individual differences quantitative or qualitative? An integrated behavioral and fMRI MIMIC approach. *Neuroimage* **202**, 116058 (2019).

34. C. J. Price, K. J. Friston, Degeneracy and cognitive anatomy. *Trends Cogn. Sci.* **6**, 416–421 (2002).

35. A. J. Anderson, *et al.*, Decoding individual identity from brain activity elicited in imagining common experiences. *Nat. Commun.* **11**, 5916 (2020).

36. A. Rokem, K. Kay, Fractional ridge regression: a fast, interpretable reparameterization of ridge regression. *Gigascience* **9** (2020).

37. J. McDermott, P. H. Schiller, J. L. Gallant, Spatial frequency and orientation tuning dynamics in area V1. *Proceedings of the* (2002).

38. V. A. Lamme, P. R. Roelfsema, The distinct modes of vision offered by feedforward and recurrent processing. *Trends Neurosci.* **23**, 571–579 (2000).

39. N. Kriegeskorte, M. Mur, P. Bandettini, Representational similarity analysis - connecting the branches of systems neuroscience. *Front. Syst. Neurosci.* **2**, 4 (2008).

40. A. Krizhevsky, I. Sutskever, G. E. Hinton, "ImageNet Classification with Deep Convolutional Neural Networks" in *Advances in Neural Information Processing Systems 25*, F. Pereira, C. J. C. Burges, L. Bottou, K. Q. Weinberger, Eds. (Curran Associates, Inc., 2012), pp. 1097–1105.

41. K. Simonyan, A. Zisserman, Very Deep Convolutional Networks for Large-Scale Image Recognition. *arXiv [cs.CV]* (2014).

42. U. Güçlü, M. A. J. van Gerven, Deep Neural Networks Reveal a Gradient in the Complexity of Neural Representations across the Ventral Stream. *J. Neurosci.* **35**, 10005–10014 (2015).

43. T. A. Carlson, D. A. Tovar, A. Alink, N. Kriegeskorte, Representational dynamics of object vision: The first 1000 ms. *J. Vis.* **13**, 1–1 (2013).

44. R. M. Cichy, D. Pantazis, A. Oliva, Resolving human object recognition in space and time. *Nat. Neurosci.* **17**, 455–462 (2014).

45. R. A. A. Ince, *et al.*, A statistical framework for neuroimaging data analysis based on mutual information estimated via a gaussian copula. *Hum. Brain Mapp.* **38**, 1541–1573 (2017).

46. B. Long, C.-P. Yu, T. Konkle, Mid-level visual features underlie the high-level categorical organization of the ventral stream. *Proc. Natl. Acad. Sci. U. S. A.* **115**, E9015–E9024 (2018).

47. N. M. Blauch, M. Behrmann, D. C. Plaut, Computational insights into human perceptual expertise for familiar and unfamiliar face recognition. *Cognition* **208**, 104341 (2021).

48. N. Abudarham, I. Grosbard, G. Yovel, Face Recognition Depends on Specialized Mechanisms Tuned to View-Invariant Facial Features: Insights from Deep Neural Networks Optimized for Face or Object Recognition. *Cogn. Sci.* **45**, e13031 (2021).

49. A. J. O'Toole, C. D. Castillo, Face Recognition by Humans and Machines: Three Fundamental Advances from Deep Learning. *Annu Rev Vis Sci* **7**, 543–570 (2021).

50. O. Parkhi, A. Vedaldi, A. Zisserman, Deep face recognition. *BMVC 2015 - Proceedings of the British Machine Vision Conference 2015* (2015) (September 2, 2023).

51. D. Cer, *et al.*, Universal Sentence Encoder. *arXiv [cs.CL]* (2018).

52. R. M. Cichy, N. Kriegeskorte, K. M. Jozwik, J. J. F. van den Bosch, I. Charest, The spatiotemporal neural dynamics underlying perceived similarity for real-world objects. *Neuroimage* **194**, 12–24 (2019).

53. M. Mur, *et al.*, Human Object-Similarity Judgments Reflect and Transcend the Primate-IT Object Representation. *Front. Psychol.* **4**, 128 (2013).

54. M. N. Hebart, B. B. Bankson, A. Harel, C. I. Baker, R. M. Cichy, The representational dynamics of task and object processing in humans. *eLife* **7** (2018).

55. J. Geskin, M. Behrmann, Congenital prosopagnosia without object agnosia? A literature review. *Cogn. Neuropsychol.* **35**, 4–54 (2018).

56. A. K. Bobak, R. J. Bennetts, B. A. Parris, A. Jansari, S. Bate, An in-depth cognitive

examination of individuals with superior face recognition skills. *Cortex* **82**, 48–62 (2016).

57. J. J. S. Barton, A. Albonico, T. Susilo, B. Duchaine, S. L. Corrow, Object recognition in acquired and developmental prosopagnosia. *Cognitive Neuropsychology* **36**, 54–84 (2019).

58. B. Duchaine, L. Germine, K. Nakayama, Family resemblance: ten family members with prosopagnosia and within-class object agnosia. *Cogn. Neuropsychol.* **24**, 419–430 (2007).

59. Y. Gabay, E. Dundas, D. Plaut, M. Behrmann, Atypical perceptual processing of faces in developmental dyslexia. *Brain Lang.* **173**, 41–51 (2017).

60. G. Jiahui, H. Yang, B. Duchaine, Developmental prosopagnosics have widespread selectivity reductions across category-selective visual cortex. *Proc. Natl. Acad. Sci. U. S. A.* **115**, E6418–E6427 (2018).

61. G. Avidan, U. Hasson, R. Malach, M. Behrmann, Detailed Exploration of Face-related Processing in Congenital Prosopagnosia: 2. Functional Neuroimaging Findings. *Journal of Cognitive Neuroscience* **17**, 1150–1167 (2005).

62. M. Behrmann, D. C. Plaut, Distributed circuits, not circumscribed centers, mediate visual recognition. *Trends Cogn. Sci.* **17**, 210–219 (2013).

63. B. C. Duchaine, G. Yovel, E. J. Butterworth, K. Nakayama, Prosopagnosia as an impairment to face-specific mechanisms: Elimination of the alternative hypotheses in a developmental case. *Cogn. Neuropsychol.* **23**, 714–747 (2006).

64. N. Furl, L. Garrido, R. J. Dolan, J. Driver, B. Duchaine, Fusiform gyrus face selectivity relates to individual differences in facial recognition ability. *J. Cogn. Neurosci.* **23**, 1723–1740 (2011).

65. J. B. Wilmer, *et al.*, Capturing specific abilities as a window into human individuality: the example of face recognition. *Cogn. Neuropsychol.* **29**, 360–392 (2012).

66. S.-M. Khaligh-Razavi, N. Kriegeskorte, Deep supervised, but not unsupervised, models may explain IT cortical representation. *PLoS Comput. Biol.* **10**, e1003915 (2014).

67. G. Jiahui, *et al.*, Modeling naturalistic face processing in humans with deep convolutional neural networks https:/doi.org/10.1101/2021.11.17.469009.

68. S. Grossman, *et al.*, Convergent evolution of face spaces across human face-selective neuronal groups and deep convolutional networks. *Nat. Commun.* **10**, 4934 (2019).

69. M. van Herten, H. H. J. Kolk, D. J. Chwilla, An ERP study of P600 effects elicited by semantic anomalies. *Brain Res. Cogn. Brain Res.* **22**, 241–255 (2005).

70. W. Shen, N. Fiori-Duharcourt, F. Isel, Functional significance of the semantic P600: evidence from the event-related brain potential source localization. *Neuroreport* **27**, 548–558 (2016).

71. M. Eimer, A. Gosling, B. Duchaine, Electrophysiological markers of covert face recognition in developmental prosopagnosia. *Brain* **135**, 542–554 (2012).

72. S. F. Popham, *et al.*, Visual and linguistic semantic representations are aligned at the border of human visual cortex. *Nature Neuroscience* **24**, 1628–1636 (2021).

73. L. Fernandino, J.-Q. Tong, L. L. Conant, C. J. Humphries, J. R. Binder, Decoding the information structure underlying the neural representation of concepts. *Proc. Natl. Acad. Sci. U. S. A.* **119** (2022).

74. S. L. Frisby, A. D. Halai, C. R. Cox, M. A. Lambon Ralph, T. T. Rogers, Decoding semantic representations in mind and brain. *Trends Cogn. Sci.* (2023) https:/doi.org/10.1016/j.tics.2022.12.006.

75. V. Bruce, A. Young, Understanding face recognition. *Br. J. Psychol.* **77 (Pt 3)**, 305–327 (1986).

76. D. Pitcher, V. Walsh, B. Duchaine, The role of the occipital face area in the cortical face perception network. *Exp. Brain Res.* **209**, 481–493 (2011).

77. J. Tardif, *et al.*, Use of face information varies systematically from developmental prosopagnosics to super-recognizers. *Psychol. Sci.* **30**, 300–308 (2019).

78. D. Anaki, S. Bentin, Familiarity effects on categorization levels of faces and objects. *Cognition* **111**, 144–149 (2009).

79. I. Gauthier, A. W. Anderson, M. J. Tarr, P. Skudlarski, J. C. Gore, Levels of categorization in visual recognition studied using functional magnetic resonance imaging. *Curr. Biol.* **7**, 645–651 (1997).

80. S. Faghel-Soubeyrand, N. Dupuis-Roy, F. Gosselin, Inducing the use of right eye enhances face-sex categorization performance. *J. Exp. Psychol. Gen.* **148**, 1834–1841 (2019).

81. J. P. Davis, K. Lander, R. Evans, A. Jansari, Investigating Predictors of Superior Face Recognition Ability in Police Super-recognisers: Superior face recognisers. *Appl. Cogn. Psychol.* **30**, 827–840 (2016).

82. M. C. Fysh, L. Stacchi, M. Ramon, Differences between and within individuals, and subprocesses of face cognition: implications for theory, research and personnel selection. *R Soc Open Sci* **7**, 200233 (2020).

83. S. Faghel-Soubeyrand, *et al.*, The two-faces of recognition ability: better face recognizers extract different physical content from left and right sides of face stimuli. *J. Vis.* **19**, 136d–136d (2019).

84. O. Langner, *et al.*, Presentation and validation of the Radboud Faces Database. *Cognition and Emotion* **24**, 1377–1388 (2010).

85. R. Kiani, H. Esteky, K. Mirpour, K. Tanaka, Object category structure in response

patterns of neuronal population in monkey inferior temporal cortex. *J. Neurophysiol.* **97**, 4296–309 (2007).

86. V. Willenbockel, *et al.*, Controlling low-level image properties: the SHINE toolbox. *Behav. Res. Methods* **42**, 671–684 (2010).

87. N. Kriegeskorte, M. Mur, N. Kriegeskorte, G. Kreiman, Representational similarity analysis of object population codes in humans, monkeys, and models. *Visual Population Codes: Towards a Common Multivariate Framework for Cell Recording and Functional Imaging* (2012).

88. R. Oostenveld, P. Fries, E. Maris, J.-M. Schoffelen, FieldTrip: Open source software for advanced analysis of MEG, EEG, and invasive electrophysiological data. *Comput. Intell. Neurosci.* **2011**, 156869 (2011).

89. M. S. Treder, MVPA-Light: A Classification and Regression Toolbox for Multi-Dimensional Data. *Front. Neurosci.* **14**, 289 (2020).

90. T. Grootswagers, S. G. Wardle, T. A. Carlson, Decoding Dynamic Brain Patterns from Evoked Responses: A Tutorial on Multivariate Pattern Analysis Applied to Time Series Neuroimaging Data. *J. Cogn. Neurosci.* **29**, 677–697 (2017).

91. R. M. Cichy, A. Oliva, A M/EEG-fMRI Fusion Primer: Resolving Human Brain Responses in Space and Time. *Neuron* (2020) https:/doi.org/10.1016/j.neuron.2020.07.001.

92. M. Graumann, C. Ciuffi, K. Dwivedi, G. Roig, R. M. Cichy, The spatiotemporal neural dynamics of object location representations in the human brain. *Nat Hum Behav* (2022) https:/doi.org/10.1038/s41562-022-01302-0.

93. J. Liu, *et al.*, Transformative neural representations support long-term episodic memory. *Sci Adv* **7**, eabg9715 (2021).

94. S. Xie, D. Kaiser, R. M. Cichy, Visual Imagery and Perception Share Neural Representations in the Alpha Frequency Band. *Curr. Biol.* **30**, 3062 (2020).

Figure captions

Figure 1. Experimental procedure. a) The histogram shows the Cambridge Face Memory Test long-form (CFMT+, (8)) scores of super-recognisers (yellow bars), typical recognisers (black bars), and an additional 332 neurotypical observers from three independent studies for comparison (77, 82, 83). **b)** Participants engaged in a one-back task while their brain activity was recorded with high-density electroencephalography. The objects depicted in the stimuli belonged to various categories, such as faces, objects, and scenes. Note that the face drawings shown here are an anonymised substitute to the experimental face stimuli presented to our participants.

Figure 2. Decoding interindividual recognition ability variations from EEG activity. a) Trial-by-trial group-membership predictions (super-recogniser or typical recogniser) were computed from EEG

patterns, for each 4-ms interval, while participants processed face (blue trace) or non-face stimuli (grey trace). Significant decoding performance occurred as early as 65 ms, peaked in the N170 window, and lasted for the remainder of the EEG epochs (p<.001). **b)** Topographies were obtained using searchlight decoding analyses, either concatenating all time points (left topographies) or for selected time-windows (right topographies). Concatenating all time points resulted in peak classification performance of 77.3% over right occipito-temporal electrodes for face and 77.5% over right occipito-temporal electrodes for non-face conditions. In the N170 window, we observed a peak classification performance of 74.8% over right-temporal electrodes for face, and 72.1% over left-temporal electrodes for non-face conditions. **c**) We decoded the CFMT+ scores of the typical recognisers using fractional ridge regression. This yielded similar results with significant decoding as early as 75 ms, peaking around the N170 time window (peak-rho_{face}=.4149, peak-$rho_{non\text{-}face}$=.4899), and lasted for the remainder of the EEG epochs (p<.01, 1K permutations, 10 repetitions).

Figure 3. Comparison of super- and typical-recogniser brain representations with those of artificial neural networks of visual and semantic processing. a) Representational dissimilarity matrices (RDM) were computed from convolutional neural networks (CNN; (40, 41) of vision, human brain activity, and a deep neural network of caption classification and sentence semantics (51). To characterise the CNN RDMs, we computed the pairwise similarity between unit activation patterns for each image independently in each CNN layer. The caption-level RDMs were derived from human caption descriptions of the images transformed into sentence embeddings. Brain RDMs were computed using cross-validated decoding performance between the EEG topographies from each pair of stimuli at every 4 ms time-point. Mutual information (45) between the model RDMs and the brain RDMs was assessed, for every participant, at each 4 ms step from stimulus onset. **b**) Mutual information between brain RDMs and AlexNet RDMs (removing shared mutual information between brain and semantic model) is shown for typical- (grey solid curve) and super-recognisers (pink solid curve). We found greater similarity with mid-level visual representations (layer 4 and 5 shown, but similar results were found for mid-layers of VGG16, another popular CNN model; see **Figure S5**) in the brains of super-recognisers (black line indicates significant contrasts, p<.05, cluster-corrected) between 133 ms and 165 ms. Similar results were observed when comparing brains and CNN models without removing the shared mutual information between brains and the semantic (caption-level) model (**Figure S5**). **c**) Mutual Information with the semantic model (excluding shared mutual information between brain and AlexNet) differed for typical- and super-recognisers in a later time window centred around 650 ms (cyan curve; super > typical, p < .05, cluster-corrected). Again, similar results were observed when comparing brains and the semantic model without removing the shared mutual information between the brain and CNN model (see **Figure S8**).

Figure 4. Linking neural representations with behavioural representations for shape, function, and semantic similarity judgements. a) Mutual information between brain RDMs and the mean RDM built from shape similarity judgements (first column) and sentence meaning similarity judgements (second column) is shown for typical- (grey curves) and super-recognisers (coloured curves). Greater similarity with shape information in the brains of super-recognisers (p<.01, uncorrected; $p\text{-corrected}_{MI}$ = .1259) and greater similarity with sentence meaning information for super-recognisers (p<.01, uncorrected; $p\text{-corrected}_{MI}$ = 0.0819) only reached significance before cluster corrections. The shaded areas of all curves represent the standard error. **b)** Conditional Mutual information between brain RDMs and the mean RDM built from similarity judgements of shape & of sentence captions meaning (removing shared mutual information between brain and sentence caption meaning RDM for shape similarity, and vice versa) is shown in typical- and super-recognisers. We found greater similarity with sentence meaning in the brains of super-recognisers between 635 ms and 787 ms (black line indicates significant contrasts, p<.05, cluster-corrected), in agreement with our comparisons with the artificial

semantic model (fig. 3b). Greater similarity with shape information in the brains of super-recognisers only reached significance before cluster corrections (p<01, uncorrected*; pcorrected$_{CMI}$ = .2098).*

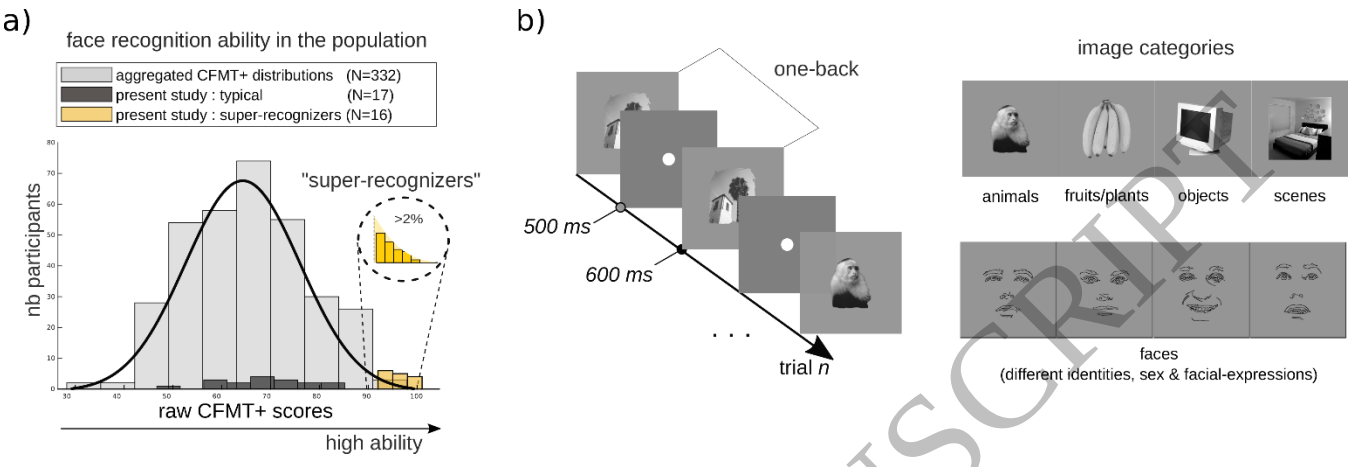

Figure 1
345x114 mm (x DPI)

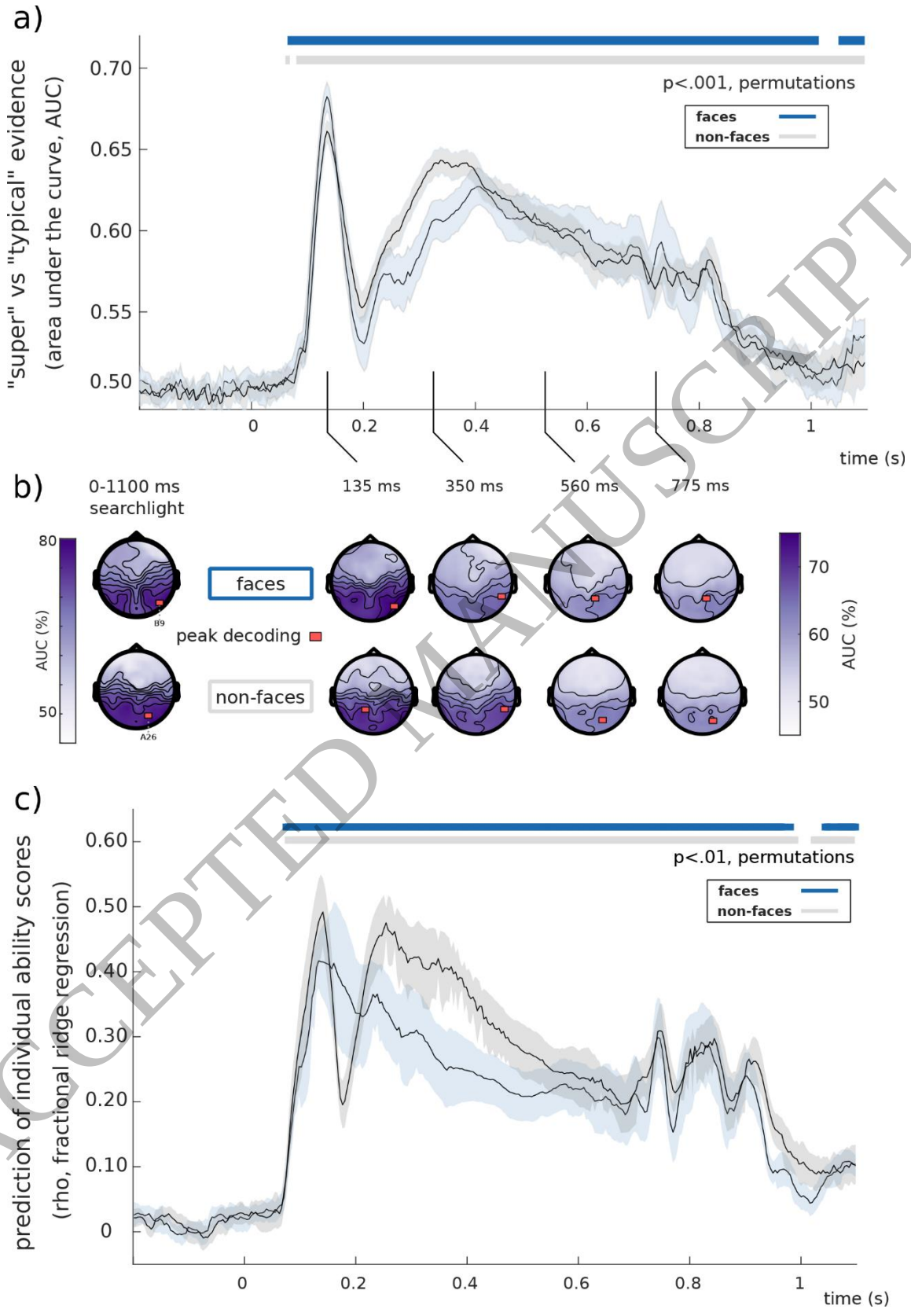

Figure 2
151x219 mm (x DPI)

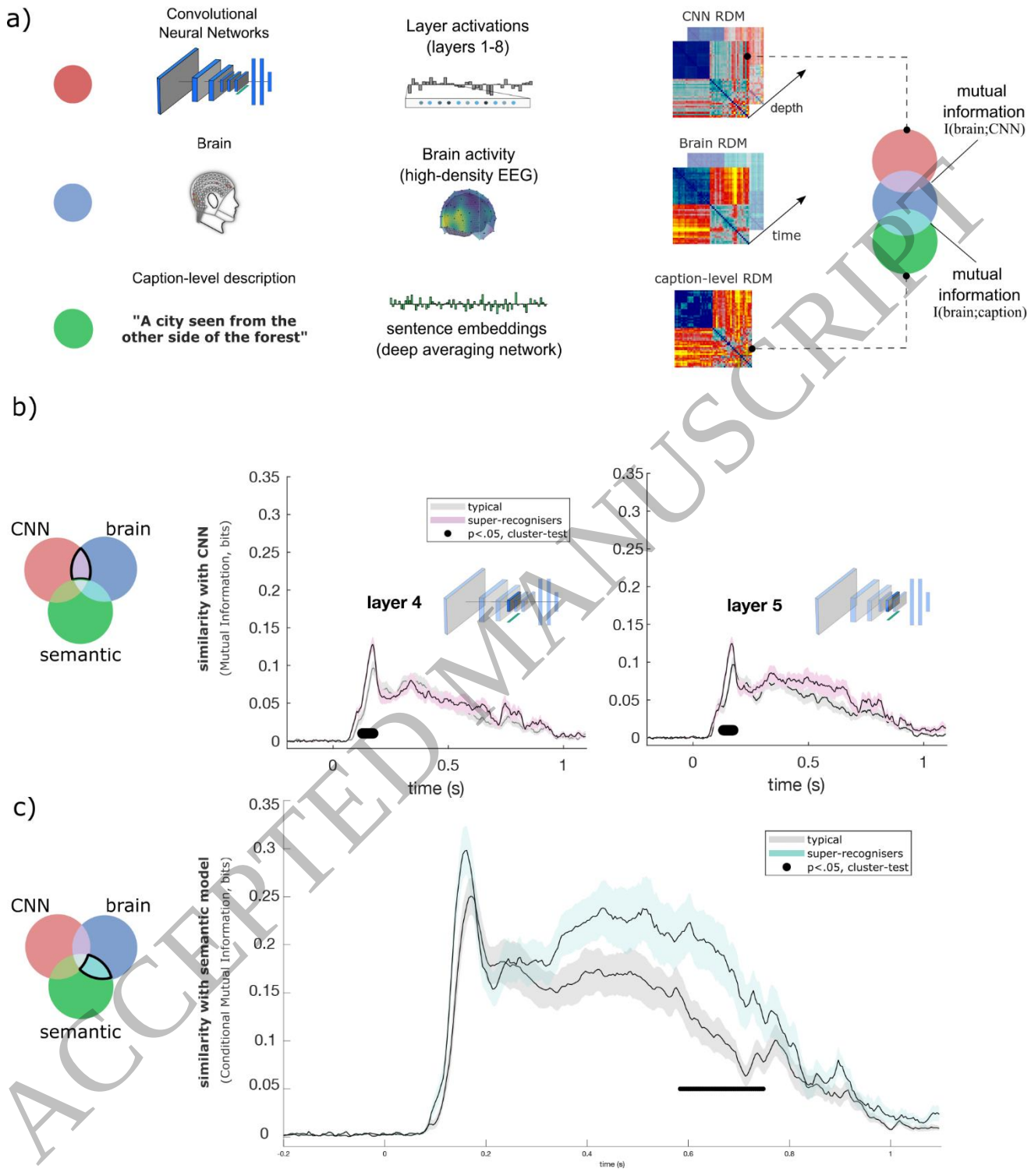

Figure 3
173x201 mm (x DPI)

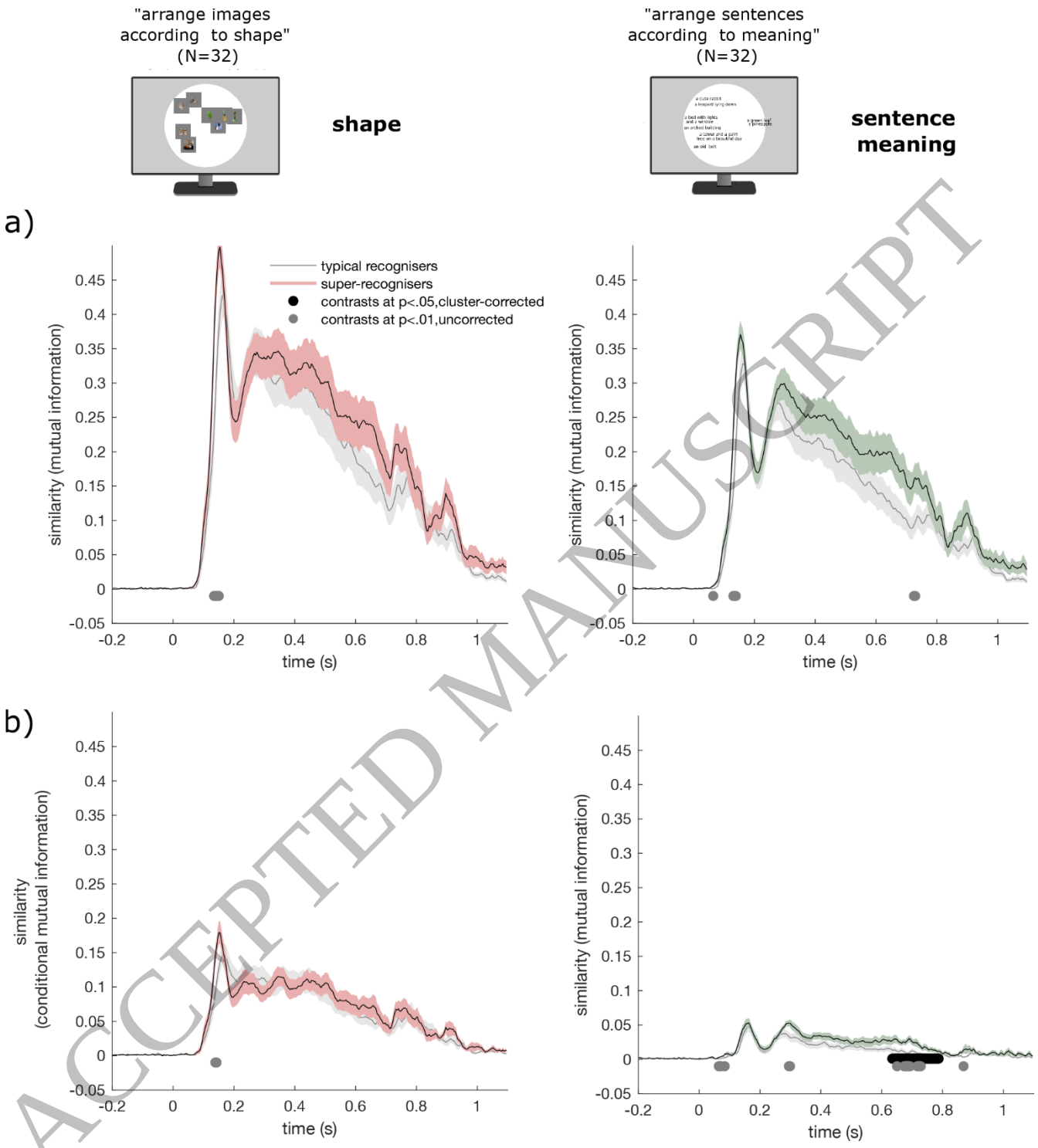

Figure 4
176x194 mm (x DPI)